International Journal of Heat and Mass Transfer 209 (2023) 124129

Contents lists available at ScienceDirect

International Journal of Heat and Mass Transfer

journal homepage: www.elsevier.com/locate/hmt

Numerical investigation on forced, natural, and mixed convective heat transfer of n-decane in laminar flow at supercritical pressures

Weitong Liu[a,b], Guoqiang Xu[a,b,c], Yanchen Fu[a,b,d,*], Jie Wen[a,b,d], Nan Zhang[e]

[a] Research Institute of Aero-engine, Beihang University, Beijing 100191, China
[b] National Key Laboratory of Science and Technology on Aero-Engine Aero-thermodynamics, Beihang University, Beijing 100191, China
[c] School of Energy and Power Engineering, Beihang University, Beijing 100191, China
[d] Beihang Hangzhou Innovation Institute Yuhang, Hangzhou, 310023, China
[e] Beijing Power Machinery Institute, Beijing 100074, China

ARTICLE INFO

Article history:
Received 29 October 2022
Revised 9 March 2023
Accepted 21 March 2023

Keywords:
Supercritical heat transfer
n-decane
Forced convection
Natural convection
Mixed convection
Nusselt number correlation

ABSTRACT

The present study numerically investigates the forced, natural, and mixed convective heat transfer characteristics of supercritical n-decane in a tube in laminar flow, focusing on the law of mutual coupling of forced and natural convection in mixed convection. Effects of heat flux (100 W/m^2–8000 W/m^2) and flow direction on heat transfer are investigated. For forced convection, deterioration occurs when the wall temperature reaches the pseudo-critical temperature and the local Nusselt number decreases by up to 17.4% compared to the theoretical value at the heat flux of 2400 W/m^2. For natural convection, heat transfer is continuously enhanced with the increase of heat flux. For mixed convection in upward flow, heat transfer is enhanced by the buoyancy of increasing the fluid velocity gradient near the wall. As for the downward flow, buoyancy illustrates the opposite effects. Based on numerical simulation results, the Nusselt number correlations are proposed for forced and natural convection respectively and the correlation for mixed convection is modeled employing a function of the forced and natural convection.

1. Introduction

The high thrust-to-weight ratio, low specific fuel consumption, and high stability are demanded in the advanced aero-engine. The turbine inlet temperature will further increase due to performance requirements, resulting in a higher thermal load. The Cooled Cooling Air (CCA) technology was proposed in the 1990s [1] and it refers to installing a heat exchanger on the aero-engine using some cold sources to pre-cool the cooling air. This method could improve the cooling quality by reducing the temperature of the cooling air.

CCA technology can be divided into two types: bypass air cooling and hydrocarbon fuel cooling. By comparison, aviation kerosene as a cold source has obvious advantages in terms of its excellent heat absorption capacity. The total heat sink of hydrocarbon fuel consists of sensible heating to raise the fuel temperature and endothermal heating caused by the chemical reaction [2]. The fuel system pressure of an aero-engine is approximately 3.4–6.5 MPa, generally higher than the critical pressure of hydrocarbon fuel. With the pressure exceeding the critical pressure, the thermophysical properties of hydrocarbon fuel hugely vary near the pseudo-critical temperature (the temperature corresponding to the peak value of specific heat). When both the temperature and pressure exceed the critical point, the fluid is at the supercritical status. Deng et al. [3–6] measured the isobaric specific heat capacity, thermal conductivity, viscosity, and density of China RP-3 aviation kerosene under supercritical pressures. As temperature increases, the thermal conductivity and dynamic viscosity decrease first and then increase slowly. The density decreases with increasing temperature and significantly decreases at the pseudo-critical temperature region. The heat transfer characteristics of supercritical fluid are always important issues in aerospace, energy, and chemical fields.

Supercritical fluids have the physical properties of both gasses and liquids. The viscosity and diffusion coefficient of supercritical fluids are close to that of gasses, while the density is like that of liquids, enabling good transport properties. Understanding the basic heat transfer characteristics of supercritical fluids is vitally important. Sun and Meng [7] conducted large eddy simulations to study upward flows and heat transfer of n-decane in a vertical tube at supercritical pressures. It is pointed out that the fluid flow and heat transfer process of supercritical n-decane with buoyancy ef-

* Corresponding author.
E-mail address: yanchenfu@buaa.edu.cn (Y. Fu).

https://doi.org/10.1016/j.ijheatmasstransfer.2023.124129
0017-9310/

Nomenclature

A	heat transfer area [m^2]
c_p	isobaric specific heat capacity [$kJ{\cdot}kg^{-1}{\cdot}K^{-1}$]
d	diameter [mm]
D	large space diameter [mm]
g	gravitational acceleration [$m{\cdot}s^{-2}$]
Gr	modified Grashof number
Gz	Graze number
h	heat transfer coefficient [$W{\cdot}m^{-2}{\cdot}K^{-1}$]
L	length [mm]
$\dot{m}$	mass flow rate [$g{\cdot}s^{-1}$]
Nu	Nusselt number
Pr	Prandtl number
P	pressure [MPa]
q	heat flux [$W{\cdot}m^{-2}$]
r	radius [mm]
Re	Reynolds number
Ra	modified Rayleigh number
T	temperature [K]
V	velocity [$m{\cdot}s^{-1}$]
x	axial distance [mm]
y	radial length [mm]

Greek symbols

α	volumetric coefficient of expansion [K^{-1}]
ρ	density [$kg{\cdot}m^{-3}$]
η	dynamic viscosity [$\mu Pa{\cdot}s$]
λ	thermal conductivity [$W{\cdot}m^{-1}{\cdot}K^{-1}$]
τ_{ij}	viscous stress tensor [$kg{\cdot}m^{-1}{\cdot}s^{-1}$]
ν	kinematic viscosity [$m^2{\cdot}s^{-1}$]

Subscripts

b	bulk
F	forced convection
in	inlet
M	mixed convection
N	natural convection
pc	pseudo-critical
W	wall
X	local position

fect can be divided into three stages. Li et al. [8] numerically investigated the flow and thermal performances of supercritical n-decane flowing in the double-layer channels. It is revealed that a cross-flow and a large vortex structure induced by the buoyancy forces are helpful to the occurrence of the heat transfer deterioration phenomenon.

Generally, the heat transfer of fluids is divided into forced, natural, and mixed convection due to the gravitational effects. The heat transfer properties of fluids for different convection were intensively investigated by researchers in the past decades [9–12]. Meyer and Everts [13] reviewed the recent developments in laminar, transitional, quasi-turbulent, and turbulent forced and mixed convective flow through horizontal tubes. It is revealed that free convection effects significantly affect the thermal entrance length, laminar-turbulent transition along the tube length, as well as the local heat transfer and pressure drop characteristics in the laminar and transitional flow regime. Tao [14] and Tyagi [15] obtained the analytic solutions for forced convective heat transfer in laminar flow using differential momentum and energy equation with some assumptions. The traditional Graetz problem of determining the temperature distribution and the Nusselt number in a channel was extended to the situation where the upper wall of the channel is non-stationary by Turkyilmazoglu [16], who generated the analytical and approximate solutions to understand the heat transfer mechanism in this case. Metais and Eckert [17] judged the influence of natural convection in mixed convection based on the Gr/Re^2 criterion. It can be regarded as forced convection when the effect of natural convection on the total heat exchange is less than 10% ($Gr/Re^2 \leq 0.1$). The heat transfer characteristics of forced convection are similar to mixed convection. The forced convective heat transfer of supercritical CO_2 in a vertical upward mini-channel was experimentally investigated by Peng et al. [18]. It is pointed out that the effects of buoyancy force acceleration perform differently under various mass fluxes.

In terms of natural convection, Wu [19] made numerical investigations of natural convective heat transfer characteristics of water in laminar flow in the tube and found that when the aspect ratio of the circular tube is relatively large, the heat transfer coefficient varies significantly with the tube diameter. Davis et al. [20] and Lee et al. [21] experimentally analyzed the natural convective heat transfer characteristics of air and CO_2 in the vertical tube and a channel formed between two vertical plates and comparative studies with the large space natural convective correlation were conducted. The natural convection of a supercritical N_2-Ar binary fluid in a long-closed vertical cylinder with an aspect ratio of 27 was conducted by Long et al. [22]. It is pointed out that the type of fluid and the geometry of the cylinder have impacts on the heat transfer characteristics of natural convection. There are three regimes in the natural convection of the supercritical N_2-Ar binary fluid with an increase in Ra: laminar thermal boundary layer regime, transition regime, and ultimate regime. Turkyilmazoglu [23] numerically investigated the process of a nonuniform wall heating within a square cavity and the resulting natural convection phenomenon by using the finite element technique. The natural convection from a vertically oriented 3-D finned tube was investigated experimentally and numerically by Ding et al. [24], who also developed a correlation of Nu for the vertically oriented 3-D finned tube.

The purely natural or forced convection correlations underestimated or overestimated the convection coefficient. Jackson et al. [25,26] experimentally studied the mixed convective heat transfer characteristics of CO_2 in a vertical tube at supercritical pressure. It is observed that the heat transfer for upward heating flow or downward cooling flow would be enhanced for laminar flow. For the opposite direction, the heat transfer can be deteriorated due to buoyancy. Nevertheless, for turbulent mixed convection, the heat transfer of downward heating is better than that of upward heating. Moreover, Jackson et al. [27] described the fluid flow and heat transfer features at supercritical pressure and concluded the basic mechanisms of heat transfer deterioration by buoyancy. Jones and Ingham [28] made numerical investigations of mixed convection between vertical parallel plates and found that when the Grashof number is relatively large, heat transfer can be enhanced if natural convection is in the opposite direction to forced convection in the central region of the flow. Nguyen et al. [29] conducted numerical studies on flow reversal and instability in mixed laminar vertical tube flow by using a full 3D-transient model and Boussinesq's assumptions. Results have shown that for the opposed-buoyancy case, flow reversal started first near the tube exit section, on the tube wall, at the level of $Gr = 3 \times 10^5$, on the tube centerline, and at the level Gr around 10^6 for assisted-buoyancy one. Research on low Reynolds number mixed convection in vertical tubes with uniform wall heat flux was carried out by Behzadmehr et al. [30]. It is revealed that there are three critical Grashof numbers for $Re = 1000$ and $Re = 1500$ in the fully developed region. Mandev and Manay [31] experimentally studied the effects of surface roughness on mixed convective heat transfer in multiple microchannels. It was observed that the effect of surface roughness on the forced convection component was more dominant compared to the natu-

Table 1
Mixed convective heat transfer coefficient correlations.

Reference	Correlation	Working Fluid	Remarks
Osborne et al. [38]	$Nu_M^3 = Nu_F^3 + Nu_N^3$	Water	Parallel plates
Lee [40]	$Nu_M^6 = Nu_F^6 + Nu_N^6$	Water	Uniformly heated vertical tube
Morcos et al. [41]	$Nu_M^2 = 4.364^2 + Nu_N^2$	Water, glycol	Horizontal tube
Mayer et al. [42]	$Nu = 4.36 + (Nu_1^6 + Nu_2^6)^{1/6}$	Water	Local Nusselt numbers for laminar flow in horizontal tube
Everts et al. [43]	$Nu = [Nu_1^{10} + (Nu_2^{-10} + Nu_3^{-10})^{-1}]^{0.1}$	Water	Average Nusselt numbers for all flow regimes in horizontal tube
Zhou et al. [44]	$Nu_M^2 = Nu_F^2 + Nu_N^2$	Surface water	For multi-row helically coiled tube heat exchanger
Qu et al. [45]	$Nu_M^2 = Nu_F^2 + Nu_N^2$	–	Packed bed
Hollingshead et al. [46]	$Nu_M^2 = Nu_F^2 + Nu_N^2$	Water	Mixed convection around two vertically aligned horizontal cylinders

ral convection component. Zhang et al. [32] conducted an experimental investigation of mixed convective heat transfer of supercritical CO_2 in downward flow, which demonstrated the occurrence of heat transfer deterioration in vertical-downward flow was mainly induced by the effect of thermal acceleration in the boundary layer.

Mixed convection is the coupling of natural convection and forced convection, and the empirical relationships of mixed convective heat transfer have drawn attention of scholars due to its extensive applications. S.V. et al. [33] proposed the Nusselt number correlations for forced, natural, and mixed convection from an isothermal horizontal plate to supercritical nitrogen by numerical method. Churchill et al. [34–37] proposed a comprehensive correlating equation modeled using a function of the forced and natural convection according to the previous works as follows:

$$\mathrm{Nu}^n = Nu_F^n + Nu_N^n \tag{1}$$

where subscripts F and N are forced convection and natural convection respectively and the power n varies with different working mediums and conditions for providing the best correlation. Obsorne et al. [38] experimentally investigated mixed convective heat transfer for transitional and turbulent flow between horizontal and parallel plates. Using the equation proposed by Churchill, Obsorne suggested the correlation for turbulent mixed convection from the bottom plates as Eq. (2) and (3).

$$Nu_H = \left[1.56 \times 10^{-5}(H/z)^{0.165} Re_H^{2.4} Pr + 0.012\left(Gr_{H,q}Pr\right)^{3/4}\right]^{1/3} \tag{2}$$

$$\frac{Nu_H}{Nu_{H,F}} = \left[1 + 769\left(\frac{z}{H}\right)^{0.165} \frac{Gr_{H,q}^{3/4}}{Re_H^{2/4} Pr^{1/4}}\right]^{1/3} \tag{3}$$

Eq. (4) for the laminar mixed convective heat transfer was used to compare with Hallman's experimental data [39] and to analyze the mixed convective heat transfer characteristics in a vertical tube under constant heat flux by Lee [40]. The form of mixed convective correlating equations suggested by Churchill is proved to be reliable and correct as listed in Table 1 [38,40-46].

$$\begin{cases} Nu^6 = Nu_F^6 + Nu_N^6 \\ Nu_F = \frac{48}{11}, Nu_N = 0.846(Ra^*)^{1/4} \text{ where } Ra^* = \frac{\rho g \beta c_p D^4}{\upsilon \alpha}\left(\frac{dT_b}{dx}\right) \end{cases} \tag{4}$$

The existing research has focused on specific and independent natural or forced convection, and there are few studies on mixed convection. What's more, little research has been carried out on the quantitative analysis of the effect proportion of natural and forced convection in mixed convection under supercritical pressures system. Considering the difficulty to eliminate the effect of natural convection in the experimental study of forced convection, especially at supercritical pressure due to the dramatic variation in density, the present study employs numerical simulations to explore the forced, natural, and mixed convective heat transfer characteristics of n-decane in laminar flow at supercritical pressures, focusing on the expression of Nusselt number correlation based on the following equation:

$$Nu_M^a = Nu_F^b + Nu_N^c \tag{5}$$

where the subscripts refer to mixed (M), forced (F), and natural (N) convection. The power a, b, and c are constants solved by fitting using numerical simulations and the forced, natural, and mixed convection are modeled in association, instead of performing special studies on individual convection types. Effects of different inlet temperatures, heat fluxes, and flow directions on the heat transfer characteristics are also investigated in this manuscript.

2. Numerical method

2.1. Physical model

Different physical models are applied according to the convection types. For forced convection, the numerical simulations were carried out under gravity-free conditions in a tube with a diameter of 5 mm, a total length of 2000 mm (400*d*), a heating section of 1800 mm (360*d*), and an adiabatic section of 200 mm (40*d*) at the outlet, as shown in Fig. 1. The tube is set up as fluid zone and the flow regime of all working conditions is laminar flow.

The large-space model is built to simulate the natural convection as shown in Fig. 2 that the vertical tube is set in the middle of the space. The length of the large space is 2000 mm and the tube in the central area of the large space is 1000 mm long. The distance from the tube exit section to the large space exit section is 750 mm. Moreover, the large space and tube are filled with fluid under gravity conditions. Fig. 3 shows the physical model of mixed convection with gravity. The inner diameter of the tube is set as 5 mm and 3 mm to cover the large range of *Gr*.

2.2. Thermal properties of n-decane

N-decane ($C_{10}H_{22}$) is selected as the working medium of this study since it has the same main component (C_{10}) as the hydrocarbon fuel and it has high-accuracy thermal parameters. The thermal properties of n-decane are obtained by the software of the NIST Reference Database [47]. The critical temperature and critical pressure of n-decane are 617.7 K and 2.103 MPa, respectively. In view of the drastic variation of the thermal properties, the properties of n-decane at 3 MPa are fitted by defining a piecewise-polynomial function of temperature based on Fig. 4.

Comparing the fitted data with the NIST data, the average absolute relative deviation of the fits for density, isobaric specific heat capacity, dynamic viscosity, and thermal conductivity is 0.03%, 0.05%, 0.71%, and 0.02%, respectively.

2.3. Governing equations

Numerous publications contain governing equations in the field of hydrodynamic and thermal. Referring to the works [48,49], the governing equations are utilized as below. ANSYS FLUENT 15.0 [50] is used as the numerical solver, and the governing equations are not made dimensionless.

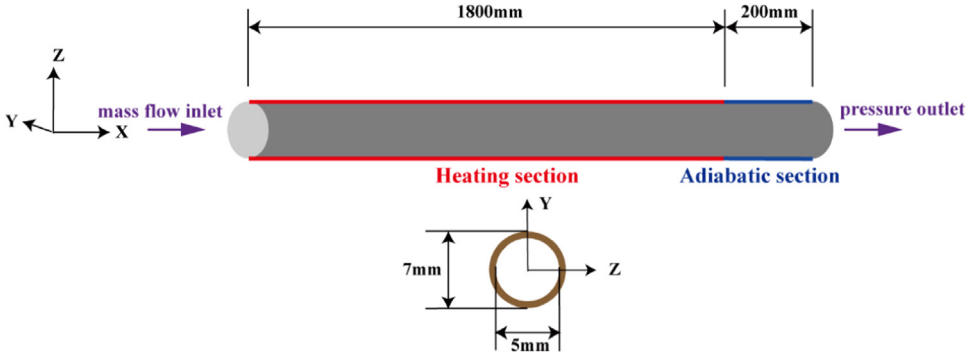

Fig. 1. Physical model of the tube for forced convection.

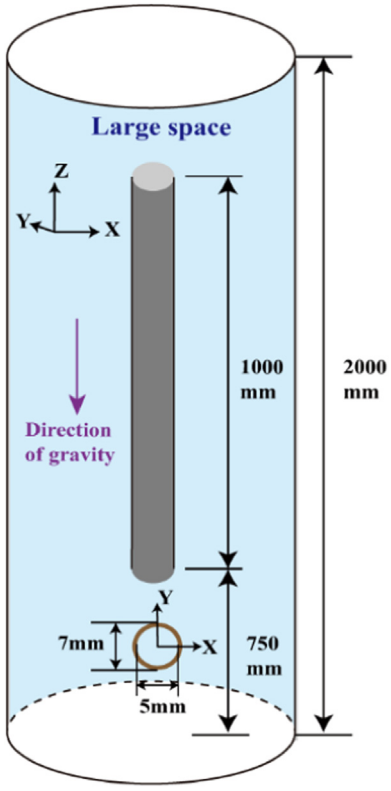

Fig. 2. Physical model of the tube for natural convection.

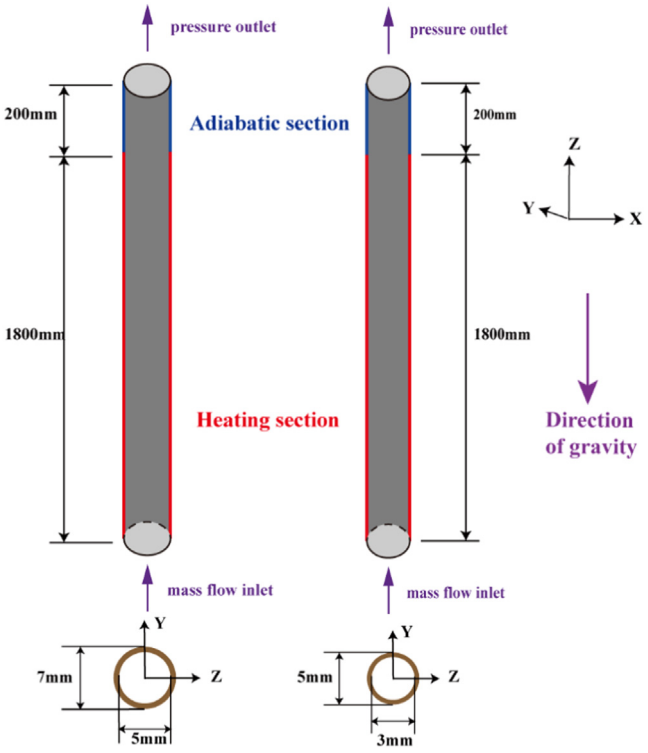

Fig. 3. Physical model of the tube for mixed convection.

Continuity equation:

$$\frac{\partial \rho}{\partial t} + \frac{\partial (\rho u_i)}{\partial x_i} = 0 \tag{6}$$

Momentum conservation equation:

$$\frac{\partial (\rho u_i)}{\partial t} + \frac{\partial \left(\rho u_i u_j\right)}{\partial x_j} = -\frac{\partial p}{\partial x_i} + \frac{\partial \tau_{ij}}{\partial x_i} + \rho f_i \tag{7}$$

f_i is the total body force and τ_{ij} is the viscous stress tensor, for Newtonian fluid, it can be obtained as follows:

$$\tau_{ij} = \eta\left(\frac{\partial u_i}{\partial x_j} + \frac{\partial u_j}{\partial x_i}\right) - \frac{2}{3}\eta\left(\frac{\partial u_k}{\partial x_k}\right)\delta_{ij} \tag{8}$$

Energy conservation equation:

$$\rho\frac{d\left(\hat{u} + u_i u_i/2\right)}{dt} = \rho f_{b,i} u_i + \frac{\partial}{\partial x_i}\left(\tau_{ij} u_j\right) + \frac{\partial}{\partial x_i}\left(\lambda\frac{\partial T}{\partial x_i}\right) + \rho\dot{q} \tag{9}$$

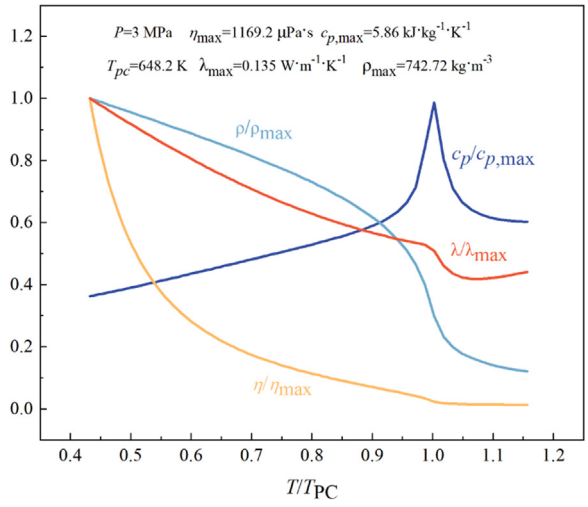

Fig. 4. Thermal properties variations with the temperature of n-decane at 3 MPa.

2.4. Numerical method

The numerical solver is ANSYS FLUENT 15.0 [50] and SIMPLEC algorithm is employed to solve the pressure-velocity coupling. Second-order upwinding is selected to discretize energy and momentum while using First order upwinding for natural convection. Moreover, the variations in the average outlet temperature and pressure are monitored. The final simulation results of all conditions ensured that the two above physical parameters remain stable.

In these simulations, the boundary conditions are similar to reality and the detailed boundary conditions are shown in the following sections. The local convective heat transfer coefficient, Nusselt number (*Nu*), Reynolds number (*Re*), Prandtl number (*Pr*), modified Grashof number (*Gr*), and modified Rayleigh number (*Ra*) of the tube are defined as below, respectively:

$$h_x = \frac{q_x}{T_{wx,in} - T_{bx}} \tag{10}$$

$$Nu_x = \frac{h_x d}{\lambda_x} \tag{11}$$

$$Re_x = \frac{4\dot{m}}{\eta_x \pi d} \tag{12}$$

$$Pr_x = \frac{\eta_x c_{px}}{\lambda_x} \tag{13}$$

$$Gr = \frac{\alpha_x g q_x d^4}{\lambda_x \nu_x^2} \tag{14}$$

$$Ra_x = Re_x Pr_x \tag{15}$$

where q_x is the wall heat flux, $T_{wx,in}$ is the inner wall temperature, T_{bx} is the mass average temperature of the tube cross-section, η_x, c_{px}, λ_x, α_x, and ν_x indicate local dynamic viscosity, specific heat, thermal conductivity, volumetric coefficient of expansion, and kinematic viscosity, respectively.

2.5. Model validations and mesh independency

2.5.1. Model validations

For fully developed forced convection laminar flow, the theoretical *Nu* is 4.364. Tyagi V et al. [15] proposed four assumptions for laminar forced convection to satisfy the analytic solutions. According to the differential form of the momentum and energy equations, we obtain the following results for the tube:

$$Nu = \frac{48}{11}\left[\left(1 + 8\frac{c_3}{c_4 a^2} + \frac{\mu c_1^2}{c_4}\right) \Big/ \left(1 + \frac{64}{11}\frac{c_3}{c_4 a^2} + \frac{5}{11}\frac{\mu c_1^2}{c_4}\right)\right] \tag{16}$$

In this equation, $8\frac{c_3}{c_4 a^2}$ and $\frac{64}{11}\frac{c_3}{c_4 a^2}$ are the internal heat source items, $\frac{\mu c_1^2}{c_4}$ and $\frac{5}{11}\frac{\mu c_1^2}{c_4}$ are the dissipative items. Since the physical model is a tube without heat-source distribution in it, the internal heat-source items can be ignored. Moreover, referring to [51], for this numerical simulation, the dissipative items can be assumed to be ignored for fully developed forced convection laminar flow. The following result can be obtained after ignoring these four items.

$$Nu = \frac{48}{11} \approx 4.364 \tag{17}$$

To verify the correctness of the physical model, the forced convection of air with constant thermal properties and variable thermal properties is calculated, respectively. The boundary conditions are listed in Table 2. The *Nu* variations along the axial direction are shown in Fig. 5. The developing section of the fluid in the tube is indicated by the vertical line before the position of $x/d = 29.8$ and its value is calculated by the Eq. (18).

$$L/d = 0.053RePr\,(\text{air}) \tag{18}$$

It is observed that there is no obvious difference in *Nu* for various heat flux conditions. In the case of constant thermal properties and $q = 36\text{W/m}^2$, the *Nu* is 4.366 for the fully developed segment, with a deviation of 0.057% from the theoretical solution. The good agreement between the simulation and theoretical results further proves the feasibility of the physical model.

To validate the physical model of natural convection, numerical results are compared with experimental data. Dyer et al. [52] experimentally investigated the heat transfer characteristics of the natural convection of air in laminar pipe flow with a constant heat flux. Fig. 6 [52] depicts the *Nu* as a function of *Ra*. The numerical simulation under the same boundary conditions is conducted according to the experimental data. By comparison, the deviation between the numerical value and the experimental value is around 8%.

2.5.2. Mesh independency

Hexahedral structured grids are used in the computational domains. An independent check of mesh is conducted before detailed investigations and the boundary conditions for all cases are listed in Table 3. For forced convection, three different grid systems with the number of 7.4×10^5, 8.4×10^5, and 1.06×10^6 are computed in the case A. Fig. 7 shows the local *Nu* variations along the axial direction and mean relative deviation among these three cases is 0.25%. This suggests that a grid system with 8.4×10^5 meshes

Table 2
Boundary conditions for forced air convection.

$\dot{m}$ [g/s]	T_{in} [K]	P [MPa]	Heat flux [W/m^2]	Thermal properties
0.01–0.05	288	0.2	36–1080	constant, variable

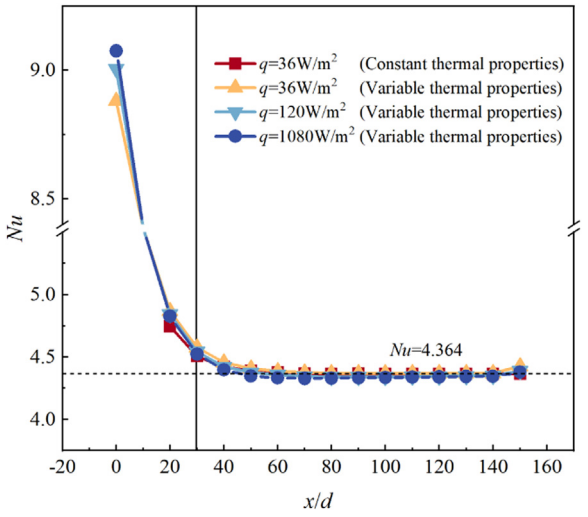

Fig. 5. Comparison of *Nu* of forced air convection as a function of dimensionless axial distance (x/d) at different heat fluxes and thermal properties conditions.

Table 3
Boundary conditions for mesh independent check.

No.	Boundary conditions	Convection type
Case A	$\dot{m} = 0.05$g/s, $Re_{in} = 685$, $T_{in} = 300$K, $P = 0.3$MPa	Forced convection
Case B	$q = 200\text{W/m}^2$, $P = 3$MPa, $T = 288$K	Natural convection

Table 4
Detailed dimensions of the large space.

No.	1	2	3
Diameter [mm]	13	14	15
Length [mm]	2000	2000	2000
Volume [mm^3]	2.65×10^5	3.05×10^5	3.53×10^5
Volume ratio	13.52	15.68	18

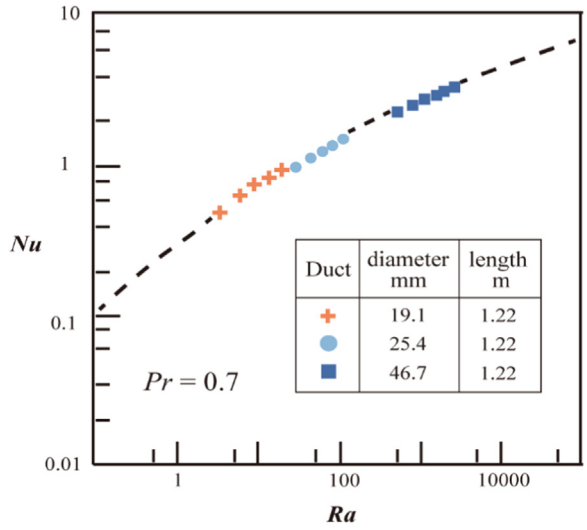

Fig. 6. Dyer [52] the relationship between *Nu* and *Ra* for the air natural convection.

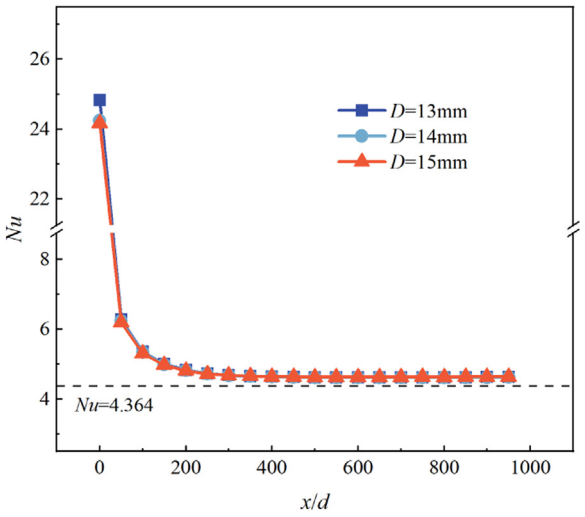

Fig. 8. Local *Nu* variations along the dimensionless axial direction (*x*/*d*) for different large space diameters.

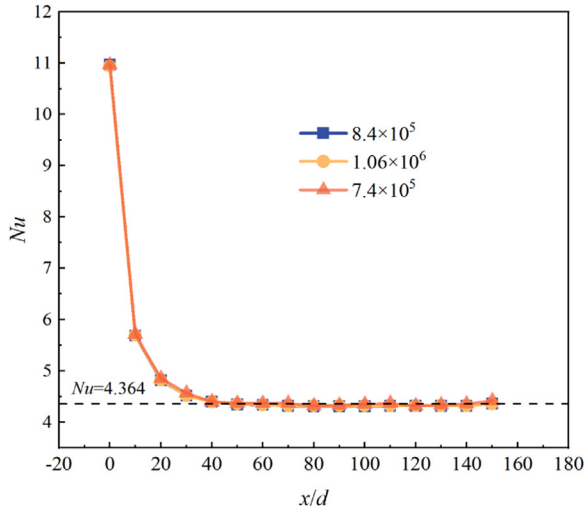

Fig. 7. Local *Nu* variations along the dimensionless axial direction (*x*/*d*) with different mesh numbers.

is appropriate and used in the following simulations of mixed and forced convection.

In terms of natural convection, the volume ratio of large space to the tube influences the heat transfer in the tube flow. Three different large space models with a large space diameter of 13 mm, 14 mm, and 15 mm are calculated in case B. The tube length in the center area of the large space is 1000 mm. The detailed dimensions of the large space are shown in Table 4. Fig. 8 displays the local *Nu* variations along the axial direction. The mean relative deviation is 0.18% and the maximum relative error is 1.7% at the inlet. Since the three large space structures have little effect on the heat transfer characteristics in the tube, selecting the large space with a diameter of 14 mm as the calculated model in the following simulations.

To verify the mesh independence of natural convection, three different grid systems with the number of 9.8×10^5, 1.16×10^6, and 1.55×10^6 are computed. Table 5 shows the mean *Nu* of different grids number. The mean relative deviation among these three cases is 0.06%. This indicates a grid system with 1.16 million meshes is enough and is employed in the following simulations.

3. Results and discussion

3.1. Forced convection

3.1.1. Effects of heat flux

The boundary conditions for forced convective numerical simulation of n-decane are shown in Table 6. Fig. 9 shows the local *Nu* variations along the axial direction with the inlet temperature of 288 K, mass flow rate of 0.4 g/s, the inlet Reynolds number of 100, and different heat fluxes. The maximum *Nu* is observed at the inlet of the tube as anticipated since the thickness of the thermal boundary layer is a minimum. Thereafter it decreases with the increasing thermal boundary layer thickness and the flow approaches fully developed flow as a theoretical *Nu* of 4.364. As can be seen from the figure, all Nusselt numbers are higher than 4.364 for fully developed flow. It could be attributed to the variable thermal properties of n-decane which are different from the theoretical derivation. As the heat flux increases, the heat transfer of n-decane in the tube is enhanced. It is the reason that as the fluid bulk temperature increases, the thermal properties of n-decane have a variation, in the near wall region, the fluid density and viscosity decrease, and the velocity gradient increases. Fig. 10 shows the velocity profiles in the fully developed segment ($x/d = 280$) of different heat fluxes. As illustrated, the velocity gradient increases in the near-wall region, and the heat transfer is enhanced.

Table 5
Mean *Nu* of different grids number.

No.	1	2	3
Grids number	9.8×10^5	1.16×10^6	1.55×10^6
Mean *Nu*	4.629	4.629	4.627

Table 6
Boundary conditions for forced convection of n-decane.

$\dot{m}$ [g/s]	Re_{in}	T_{in} [K]	P [MPa]	Heat flux [W/m^2]	Thermal properties
0.2–0.4	50–570	288, 373, 473	3	1000–8000	Variable

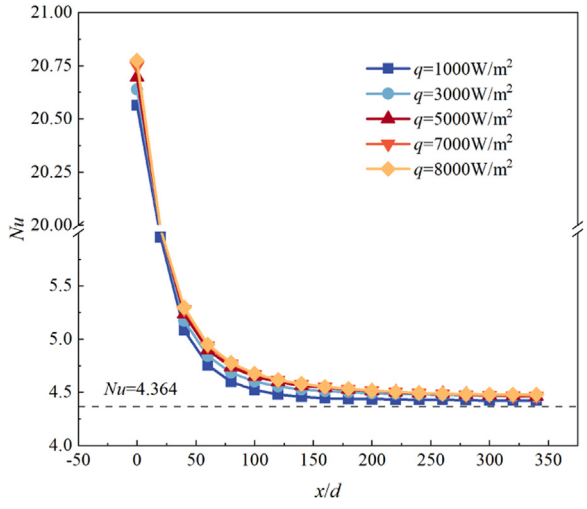

Fig. 9. Local *Nu* variations along the dimensionless axial direction (x/d) at different heat fluxes for forced convection.

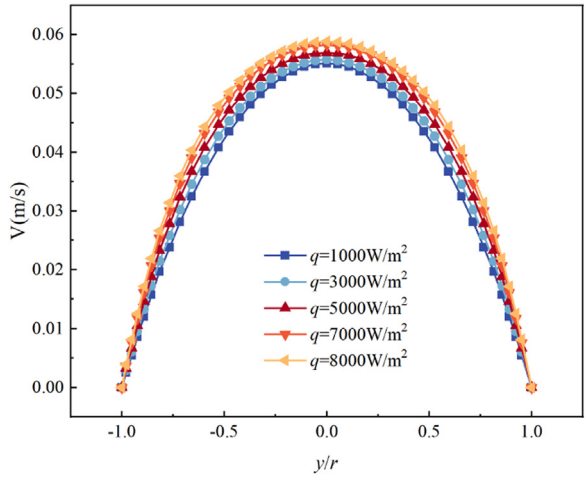

Fig. 10. Velocity profiles of different heat fluxes in the fully developed segment (x/d = 280) for forced convection.

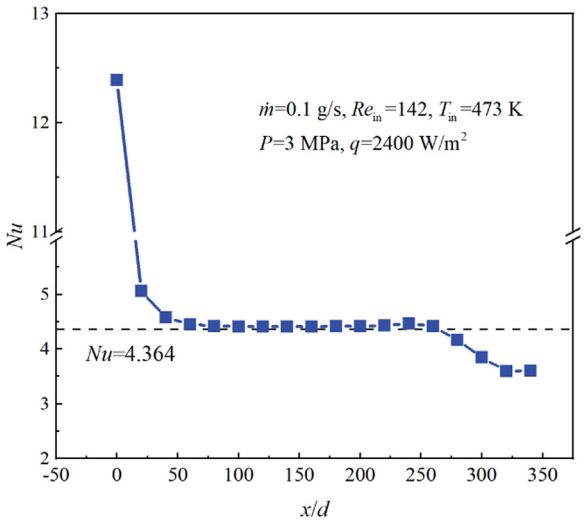

Fig. 11. Local *Nu* variations along the dimensionless axial direction (x/d) for forced convection.

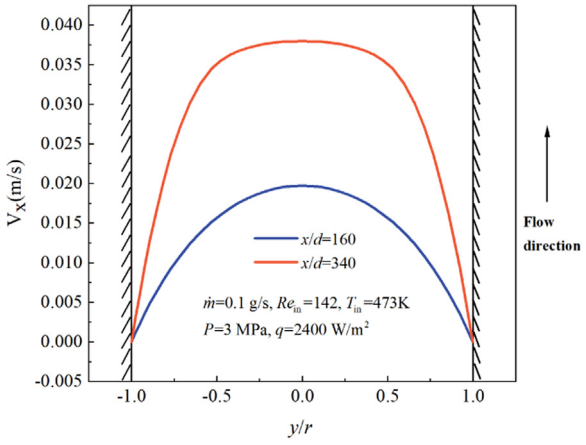

Fig. 12. Velocity profiles at the normal heat transfer section (x/d = 160) and heat transfer deterioration section (x/d = 340) for forced convection.

3.1.2. Heat transfer deterioration

Fig. 11 depicts that local *Nu* increases slowly along the flow direction in the fully developed segment and reaches the peak value at the location of x/d = 240 where the near-wall fluid temperature comes to the pseudo-critical temperature under conditions of mass flow rate 0.1 g/s, inlet temperature 473 K and heat flux 2400 W/m^2. As the fluid continues to be heated and the fluid temperature continues to rise, heat transfer deterioration occurs. At the location of x/d = 340, the local *Nu* is 3.604, decreased by 17.4% compared to the theoretical value at the heat flux of 2400 W/m^2.

Figs. 12 and 13 show the velocity profile and temperature profile for the normal heat transfer section (x/d = 160) and the heat transfer deterioration section (x/d = 340), respectively. As shown in the figure, in the region of $0.48<|y/r|<1$, the fluid temperature exceeds the pseudo-critical temperature and the fluid reaches the supercritical state. The density and viscosity of the fluid near the wall dramatically decrease, resulting in an acceleration of the fluid near the wall and the increase of the velocity gradient, which promotes heat transfer. However, the thermal conductivity of n-decane rapidly decreases in this region which inhibits heat trans-

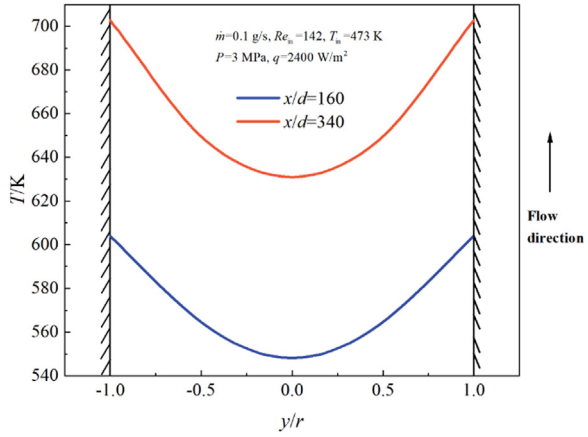

Fig. 13. Temperature profiles at the normal heat transfer section (x/d = 160) and heat transfer deterioration section (x/d = 340) for forced convection.

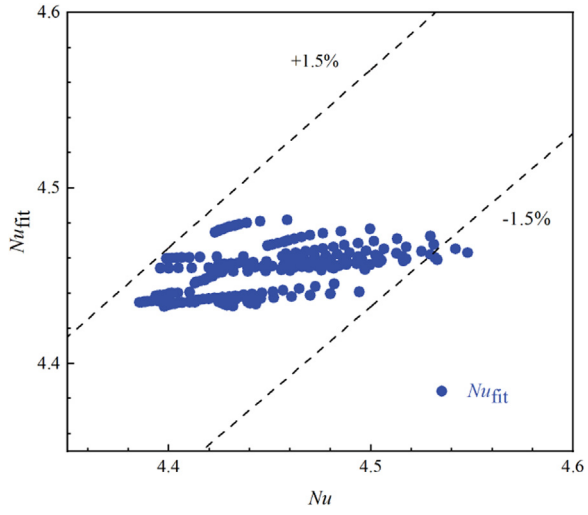

Fig. 14. Comparison between the numerical simulation values and the fitting correlation calculation values for forced convection.

fer. Compared to the normal heat transfer section, although the near-wall fluid in the heat transfer deterioration section has a large velocity gradient and can promote heat transfer, the velocity gradient of the fluid in the central area is small. Since there is no mixing between the layers in laminar flow, heat transfer relies on the momentum exchange between the layers, so the excessive small velocity gradient in the central region would seriously deteriorate the heat transfer. In contrast to laminar flow, heat transfer is enhanced when the flow regime is turbulent and the fluid temperature reaches the pseudo-critical temperature.

3.1.2. Correlation for forced convection

On basis of the numerical simulation data, the fitting correlation of forced convective heat transfer of n-decane in the tube at supercritical pressure is gained as follows by implementing a least squares method.

$$Nu = 4.364 + 0.00266Re^{0.3328}Pr^{0.8243} \quad (19)$$

where $4.16<Pr<16$. To check the accuracy of the correlation of forced convection, a comparison with the numerical data is displayed in Fig. 14. 96% of points have ±1.5% deviation, indicating that the correlation has relatively high fitting accuracy.

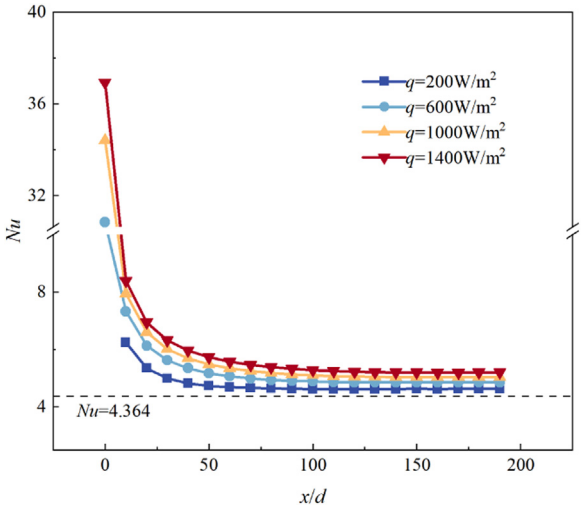

Fig. 15. Local Nu variations along the dimensionless axial direction (x/d) at different heat fluxes for natural convection.

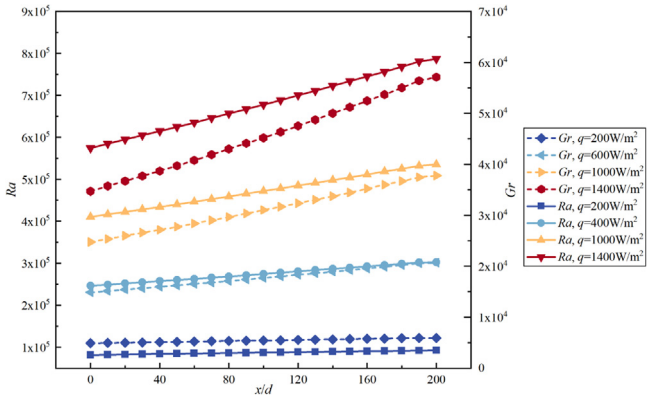

Fig. 16. Local Ra and Gr variation along the dimensionless axial direction (x/d) at different heat fluxes.

3.2. Natural convection

3.2.1. Effects of heat flux

The boundary conditions for the natural convective numerical simulation of n-decane are listed in Table 7. Fig. 15 shows the local Nu variations along the axial direction with a large space temperature field of 288 K and different heat fluxes (200–1400 W/m^2). As illustrated, natural convection is caused by the density difference due to the temperature increase of the fluid. Moreover, there is a developing section in the tube with a thin thermal boundary layer in the inlet section where the local heat transfer coefficient is large. With the development of the flow boundary layer and thermal boundary layer, the local heat transfer coefficient is stable along the flow direction. As the heat flux increases, the natural convective heat transfer of n-decane at supercritical pressure is continuously enhanced. The local Ra and Gr variations along the axial direction at different heat fluxes are shown in Fig. 16. According to previous research, the regime of natural convection in the case of q = 200–1400 W/m^2 and $Ra = 8 \times 10^4$–8×10^5 is laminar. It is clearly found that the local Ra and Gr increase with the increasing heat flux and the natural convection effects are enhanced by buoyancy.

3.2.2. Correlation for natural convection

In terms of the numerical simulation values, the fitting correlation of natural convective heat transfer of n-decane at supercritical

Table 7
Boundary conditions for natural convection of n-decane.

$\dot{m}$ [g/s]	T_c [K]	P [MPa]	Heat flux [W/m^2]	Tube inner diameter [mm]
0.2–0.4	288–473	3	100–5000	3, 5

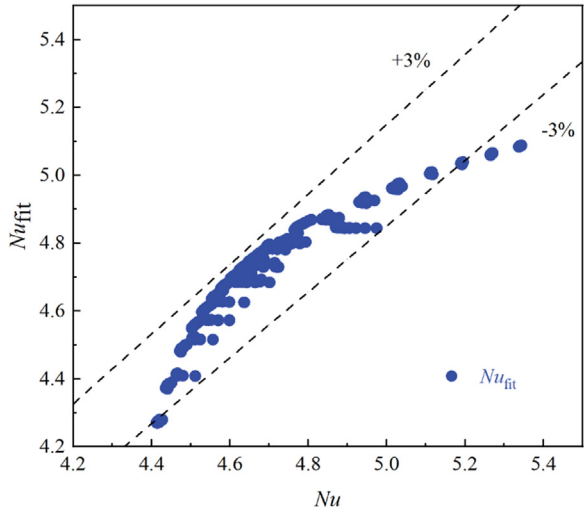

Fig. 17. Comparison between the numerical simulation values and the fitting correlation values for natural convection.

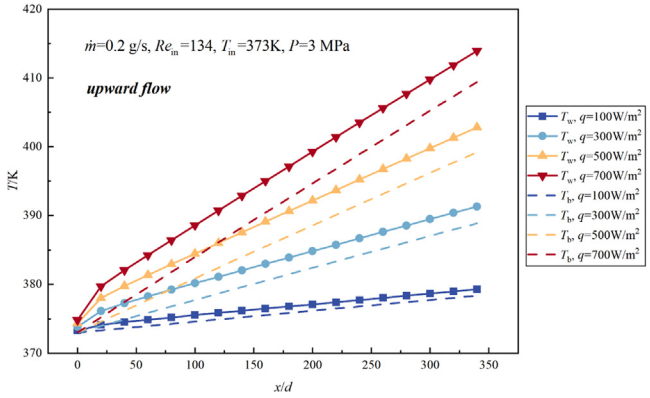

Fig. 18. Temperature variations along the dimensionless axial direction (x/d) at different heat fluxes for mixed convection.

pressure is obtained as follows through the least squares method.

$$Nu = 2.981 \times Ra^{0.0343} \times Pr^{0.0229} \quad (20)$$

where $350<Gr<1.7 \times 10^5$, $5<Pr<16$. Fig. 17 presents a comparison between the numerical simulation values and the fitting correlation values. As shown in the figure, 94% of points with ±3% deviation, implying the correlation of Eq. (20) can accurately predict Nu for natural convection.

3.3. Mixed convection

3.3.1. Effects of flow direction and heat flux

Fig. 18 demonstrates the wall temperature (T_w) and bulk temperature (T_b) vary axially from the tube inlet at different heat fluxes. N-decane flows upward in the tube and all boundary conditions of mixed convection are enumerated in Table 8. Fig. 19 summarizes the local Nu as a function of axial position x/d for upward flow at different heat fluxes. Similarly, the inlet region is the developing section of the boundary layer, where the heat transfer coefficient is large, and T_w and T_b grow quickly with a large slope. When the flow is simultaneously hydrodynamically and thermally developed, Nu varies slowly along the flow direction, and T_w and T_b tend to increase linearly along the course.

Table 8
Boundary conditions for mixed convection of n-decane.

$\dot{m}$ [g/s]	0.1, 0.2, 0.4
Re_{in}	25–570
T_{in} [K]	288–473
P [MPa]	3
Heat flux [W/m^2]	100–4900
Tube inner diameter [mm]	3, 5
Flow direction	Upward and downward

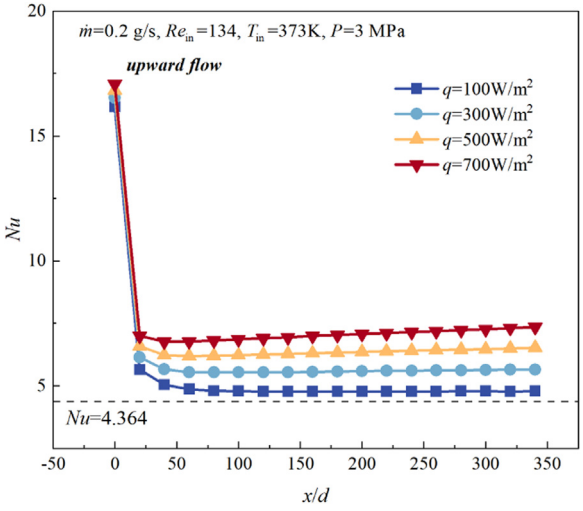

Fig. 19. Local Nu variations along the dimensionless axial direction (x/d) at different heat fluxes for mixed convection.

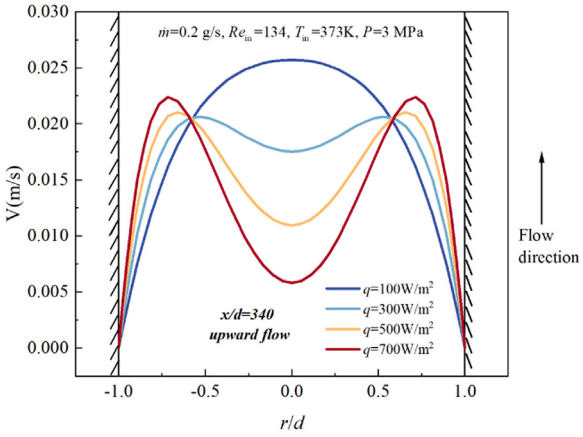

Fig. 20. Velocity profiles of different heat fluxes at the location of x/d = 340 for mixed convection.

Fig. 20 displays the mixed convective velocity profile of n-decane for upward flow. When heat flux is 100 W/m^2, the velocity profile is parabolic. As the heat flux increases, the fluid velocity in the central region gradually decreases, the fluid velocity

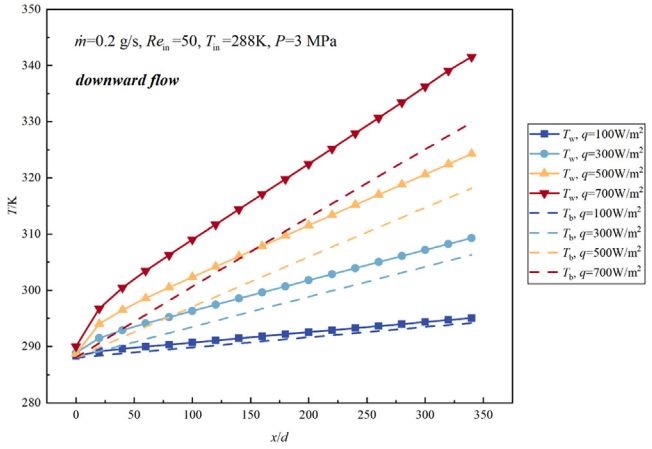

Fig. 21. Temperature variations along the dimensionless axial direction (x/d) at different heat fluxes for mixed convection.

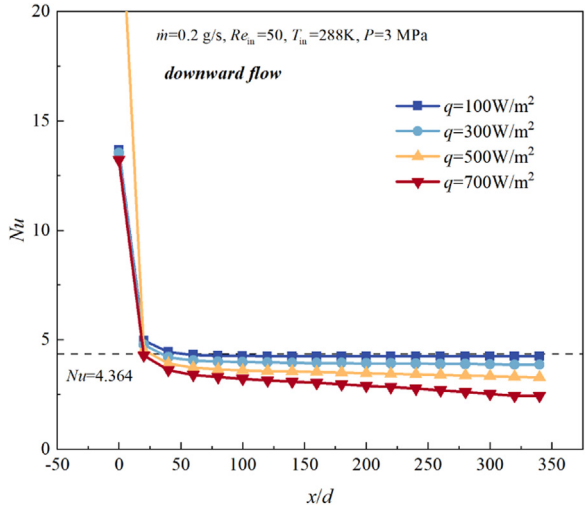

Fig. 22. Local Nu variations along the dimensionless axial direction (x/d) at different heat fluxes for mixed convection.

near the wall gradually increases, and the velocity profile is M-shaped. The increased velocity gradient of the fluid near the wall leads to an enhanced heat transfer capacity and increases the heat transfer coefficient. The main reason for this phenomenon is that when flowing upwards, the fluid temperature increases by heating, and the uneven temperature field in the radial direction produces an uneven density field. Thus, natural convection occurs because of buoyancy. Since buoyancy is upward, in the same direction as forced convection, it promotes heat transfer and increases the heat transfer coefficient.

Figs. 21 and 22 demonstrate T_w and T_b and local Nu variations of different heat fluxes for downward flow. Compared with the upward flow, the local Nu decreases slowly in the fully developed section. However, for turbulent mixed convection, buoyancy illustrates the opposite effects. When fluid flows upwards, the localized heat transfer deterioration occurs due to buoyancy reducing the shear stress in the wall layer region. Therefore, the production of turbulence will be lower and heat transfer is impaired. When fluid flows downwards, the shear stress in the wall layer region is larger than the upward flow, promoting the production of turbulence to enhance heat transfer [27].

Fig. 23 shows the mixed convective velocity profile of n-decane for upward flow. When heat flux is 100 W/m^2, the velocity profile is parabolic. As shown in Fig. 23, the fluid velocity in the central

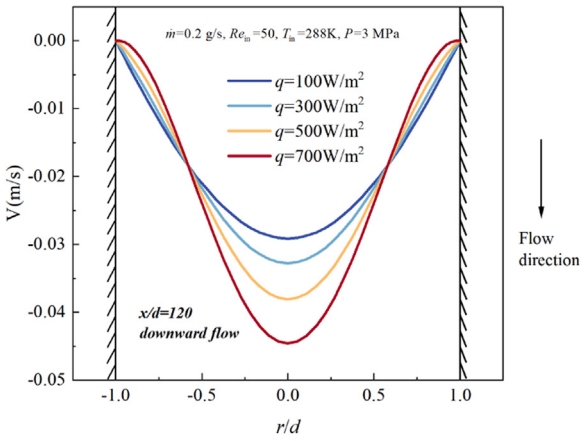

Fig. 23. Velocity profiles of different heat fluxes at the location of x/d = 120 for mixed convection.

Table 9
Values of the coefficients for upward flow.

Ra	a	b	c	d	Average fitting relative error [%]
$<5 \times 10^5$	9.76	2.75	9.39	1.17	3.94
5×10^5–10^6	12.33	2.75	12.88	12.02	5.82
$>10^6$	12.33	2.75	12.97	11.61	6.79

region continues to accelerate with the heat flux increasing, the fluid velocity near the wall slows down and the velocity gradient decreases. Due to the reduction of the fluid velocity gradient near the wall, the momentum exchange between the layers is weakened and the heat transfer coefficient is reduced. Since the direction of the buoyancy force is upward, while the direction of flow is downward, the direction of natural convection is opposite to the direction of forced convection. Therefore, under the impact of buoyancy, the velocity gradient of the fluid near the wall is reduced, weakening the heat transfer.

3.3.2. Correlation for mixed convection

Compared to the studies of purely forced or natural convection, it is of practical interest to employ some simple formulas to develop the correlation of mixed convection due to the complex cross-flow and buoyancy-induced flow mixing [44]. On basis of the correlation between forced and natural convection of n-decane in the tube at supercritical pressure obtained in Section 3.1.2 and Section 3.2.2, combining the calculated data of mixed convection in Section 3.3.1, the Nu of mixed convection can be correlated well by Eq. (21) and the values of a, b, c in the equation can be solved using the least squares method. The plus and minus signs refer to the upward flow and downward flow, respectively.

$$Nu_M = \left(Nu_F^a \pm Nu_N^b\right)^{1/c} \cdot \left(\frac{\mu_w}{\mu_b}\right)^d \tag{21}$$

Where

$$Nu_F = 4.364 + 0.002662 \times Re^{0.332793} \times Pr^{0.824303} (4.16 < Pr < 16) \tag{22}$$

$$Nu_N = 2.981 \times Ra^{0.0343} \times Pr^{0.0229} (350 < Gr < 1.7 \times 10^5, 5 < Pr < 16) \tag{23}$$

Tables 9 and 10 enumerate the values of the coefficients in the empirical correlation for upward and downward flow, respectively. The values of each coefficient of the correlation vary based on Ra

Table 10
Values of the coefficients for downward flow.

Ra	a	b	c	d	Average fitting relative error [%]
$<10^5$	3.24	2.46	3.6	0.01	0.8
10^5–10^6	2.09	1.76	1.38	0	3.12
$>10^6$	3.69	3.35	2.66	0	6.92

ranges. Lee J et al. [40] suggested Eq. (4) for the laminar mixed convection for uniformly heated vertical tube, where the coefficients a, b, and c in Eq. (21) are all equal to 6. Mayer J and Everts M [42] proposed Eq. (24) to calculate the local *Nu*, which combined the equation for the forced convection developing region (Nu_1) and combined mixed convection developing and fully developed regions (Nu_2). The coefficients a, b, and c in Eq. (24) are also equal to 6. Compared to the previous works with the present results shown in Tables 9 and 10, mixed convective heat transfer of n-decane in laminar flow at supercritical pressures is more complicated. In Eq. (21), the coefficients a, b, and c all differ from one another. Not only is it influenced by the flow direction, but the dynamic viscosity also has an impact on the correlation.

$$\begin{cases} Nu = 4.36 + \left(Nu_1^6 + Nu_2^6\right)^{1/6} \\ Nu_1 = \left(0.33Gz^{0.54} - 0.84\right)Pr^{-0.2} \\ Nu_2 = \left(0.207Gr^{0.305} - 1.19\right)Pr^{0.5}Gz^{-0.08} \end{cases} \tag{24}$$

According to a determined mixed convection condition, the *Nu* of mixed convection and the *Re*, *Pr*, and *Gr* of this condition are known, and the *Nu* of forced convection and the *Nu* of natural convection can be calculated. Moreover, the actual measurements are all mixed convection cases, so the specific proportion of the two cannot be analyzed exactly under experimental conditions. With Eq. (21), it is convenient to analyze the inter-coupling law of forced convection and natural convection under mixed convection and reveal the heat transfer characteristics of mixed convection.

4. Conclusion

The forced, natural, and mixed convective heat transfer characteristics of n-decane in a tube in laminar flow at supercritical pressures are investigated in the present study, focusing on the law of mutual coupling of forced and natural convection in mixed convection. The main conclusions are summarized as follows.

- For laminar flow in the tube of n-decane at supercritical pressure, heat transfer deterioration occurs when the fluid temperature near the wall exceeds the pseudo-critical temperature. When the bulk fluid temperature completely reaches the pseudo-critical temperature, heat transfer would be enhanced.
- For mixed convection in laminar flow, buoyancy would change the velocity profile in the tube. For the upward flow, buoyancy will increase the velocity gradient of the fluid near the wall, producing an M-shaped velocity profile and enhancing heat transfer. For the downward flow, buoyancy will decrease the velocity gradient of the fluid near the wall, weakening the heat transfer.
- The *Nu* fitting correlations with high accuracy of supercritical n-decane for forced, natural and mixed convection in laminar flow are proposed.
- The quantitative analysis of the effect proportion of natural and forced convection in mixed convection under supercritical pressures system can be carried out by using the proposed *Nu* fitting formulas. Generally, it is considered that the effects of forced convection are normally greater than the natural convective ones in mixed convection. However, as the heat flux continues to increase, the effects of natural convection become more pronounced. The specific quantified proportions can be obtained by the proposed correlations for the studied conditions.

Declaration of Competing Interest

The authors declared that they have no conflicts of interest to this work.

CRediT authorship contribution statement

Weitong Liu: Formal analysis, Investigation, Data curation, Writing – original draft. **Guoqiang Xu:** Conceptualization, Project administration. **Yanchen Fu:** Methodology, Writing – review & editing. **Jie Wen:** Supervision. **Nan Zhang:** Resources.

Data Availability

Data will be made available on request.

Acknowledgment

The authors appreciate the supports from the National Science and Technology Major Project of China (Nos. 2017-III-0005-0029, J2019-III-0021-0065, and J2019-III-0015-0059), the Fundamental Research Funds for the Central Universities, and the Science Center for Gas Turbine Project (P2022-C-II-005-001).

References

[1] G.B. Bruening, W.S. Chang, Cooled Cooling Air Systems For Turbine Thermal management, in: Turbo Expo: Power for Land, Sea, and Air, American Society of Mechanical Engineers, 1999 V003T001A002.
[2] H. Huang, L.J. Spadaccini, D.R. Sobel, Fuel-cooled thermal management for advanced aeroengines, J. Eng. Gas Turbines Power 126 (2) (2004) 284–293.
[3] H. Deng, K. Zhu, G. Xu, Z. Tao, C. Zhang, G. Liu, Isobaric specific heat capacity measurement for kerosene RP-3 in the near-critical and supercritical regions, J. Chem. Eng. Data 57 (2) (2012) 263–268.
[4] G. Xu, Z. Jia, J. Wen, H. Deng, Y. Fu, Thermal-conductivity measurements of aviation kerosene RP-3 from (285 to 513) K at sub-and supercritical pressures, Int. J. Thermophys. 36 (4) (2015) 620–632.
[5] H. Deng, C. Zhang, G. Xu, B. Zhang, Z. Tao, K. Zhu, Viscosity measurements of endothermic hydrocarbon fuel from (298 to 788) K under supercritical pressure conditions, J. Chem. Eng. Data 57 (2) (2012) 358–365.
[6] H. Deng, C. Zhang, G. Xu, Z. Tao, B. Zhang, G. Liu, Density measurements of endothermic hydrocarbon fuel at sub-and supercritical conditions, J. Chem. Eng. Data 56 (6) (2011) 2980–2986.
[7] X. Sun, H. Meng, Large eddy simulations and analyses of hydrocarbon fuel heat transfer in vertical upward flows at supercritical pressures, Int. J. Heat Mass Transf. (2021) 170.
[8] Y. Li, G. Xie, B. Sunden, Flow and thermal performance of supercritical n-decane in double-layer channels for regenerative cooling of a scramjet combustor, Appl. Therm. Eng. (2020) 180.
[9] M. Turkyilmazoglu, Heat absorption due to falling film with imposed uniform mass fraction at the wall, Int. J. Heat Mass Transf. 177 (2021) 121585.
[10] S.R.G. Polasanapalli, K. Anupindi, Mixed convection heat transfer in a two-dimensional annular cavity using an off-lattice Boltzmann method, Int. J. Therm. Sci. 179 (2022) 107677.
[11] M. Habibishandiz, Z. Saghir, MHD mixed convection heat transfer of nanofluid containing oxytactic microorganisms inside a vertical annular porous cylinder, Int. J. Thermofluid. 14 (2022) 100151.
[12] L. Yang, K. Du, A comprehensive review on the natural, forced, and mixed convection of non-Newtonian fluids (nanofluids) inside different cavities, J. Therm. Anal. Calorim. 140 (2020) 2033–2054.
[13] J.P. Meyer, M. Everts, A review of the recent developments in laminar, transitional, quasi-turbulent and turbulent forced and mixed convective flow through horizontal tubes, Adv. Heat Transf. 51 (2019) 131–205.
[14] L. Tao, On some laminar forced-convection problems, (1961).
[15] V. Tyagi, Laminar forced convection of a dissipative fluid in a channel, (1966).
[16] M. Turkyilmazoglu, Heat transport in shear-driven flow with axial conduction, J. Taiwan Inst. Chem. Eng. 123 (2021) 96–103.
[17] B. Metais, E. Eckert, Forced, mixed, and free convection regimes, (1964).
[18] R. Peng, X. Lei, Z. Guo, Y. Wang, H. Li, X. Zhou, Forced convective heat transfer of supercritical carbon dioxide in mini-channel under low mass fluxes, Int. J. Heat Mass Transf. (2022) 182.
[19] Y. Wu, Laminar natural convection in vertical tubes with one end open to a large reservoir, (1995).

[20] L.P. Davis, J.J. Perona, Development of free convection flow of a gas in a heated vertical open tube, Int. J. Heat Mass Transf. 14 (7) (1971) 889–903.
[21] T. Lee, P. Parikh, A. Acrivos, D. Bershader, Natural convection in a vertical channel with opposing buoyancy forces, Int. J. Heat Mass Transf. 25 (4) (1982) 499–511.
[22] Z.Q. Long, P. Zhang, B. Shen, Natural convection heat transfer of supercritical binary fluid in a long closed vertical cylinder, Int. J. Heat Mass Transf. 80 (2015) 551–561.
[23] M. Turkyilmazoglu, Exponential nonuniform wall heating of a square cavity and natural convection, Chin. J. Phys. 77 (2022) 2122–2135.
[24] Y. Ding, W. Zhang, B. Deng, Y. Gu, Q. Liao, Z. Long, X. Zhu, Experimental and numerical investigation on natural convection heat transfer characteristics of vertical 3-D externally finned tubes, Energy 239 (2022) 122050.
[25] J. Jackson, M. Cotton, B. Axcell, Studies of mixed convection in vertical tubes, Int. J. Heat Fluid Flow 10 (1) (1989) 2–15.
[26] W.B. Hall, J. Jackson, Laminarization of a turbulent pipe flow by buoyancy forces, Mechanical Engineering 10017 (1969) pp. 66-&.
[27] J.D. Jackson, Fluid flow and convective heat transfer to fluids at supercritical pressure, Nucl. Eng. Des. 264 (2013) 24–40.
[28] A. Jones, D. Ingham, Flow reversal in a combined convection flow of Newtonian fluid in a vertical duct, Acta Mech. 99 (1–4) (1993) 135–153.
[29] C.T. Nguyen, S.E.B. Maïga, M. Landry, N. Galanis, G. Roy, Numerical investigation of flow reversal and instability in mixed laminar vertical tube flow, Int. J. Therm. Sci. 43 (8) (2004) 797–808.
[30] A. Behzadmehr, N. Galanis, A. Laneville, Low Reynolds number mixed convection in vertical tubes with uniform wall heat flux, Int. J. Heat Mass Transf. 46 (25) (2003) 4823–4833.
[31] E. Mandev, E. Manay, Effects of surface roughness in multiple microchannels on mixed convective heat transfer, Appl. Therm. Eng. 217 (2022) 119102.
[32] S. Zhang, X. Xu, C. Liu, X. Li, C. Wu, C. Dang, Experimental investigation and theoretical analysis on the heat transfer deterioration of supercritical CO2 in mixed and forced convection in vertical-straight tube with downward flow, Int. J. Heat Mass Transf. (2022) 187.
[33] S.V. SSS, R. Ranganath, S. Shaju, T.R. Seetharam, K.N. Seetharamu, Numerical predictions of forced convection and free convection heat transfer from an isothermal horizontal flat plate to supercritical nitrogen, Therm. Sci. Eng. Progr. (2021) 23.
[34] S.W. Churchill, Laminar free convection from a horizontal cylinder with a uniform heat flux density, Lett. Heat Mass Transf. 1 (2) (1974) 109–111.
[35] S.W. Churchill, H.H. Chu, Correlating equations for laminar and turbulent free convection from a vertical plate, Int. J. Heat Mass Transf. 18 (11) (1975) 1323–1329.
[36] S.W. Churchill, H. Ozoe, Correlations for laminar forced convection with uniform heating in flow over a plate and in developing and fully developed flow in a tube, (1973).
[37] S.W. Churchill, A comprehensive correlating equation for laminar, assisting, forced and free convection, AIChE J. 23 (1) (1977) 10–16.
[38] D. Osborne, F. Incropera, Experimental study of mixed convection heat transfer for transitional and turbulent flow between horizontal, parallel plates, Int. J. Heat Mass Transf. 28 (7) (1985) 1337–1344.
[39] T.M. Hallman, Experimental Study of Combined Forced and Free-laminar Convection in a Vertical Tube, National Aeronautics and Space Administration, 1961.
[40] J. Lee, The Flow Structure Under Mixed Convection in a Uniformly Heated Vertical Pipe, Massachusetts Institute of Technology, 2005.
[41] S. Morcos, A. Bergles, Experimental investigation of combined forced and free laminar convection in horizontal tubes, (1975).
[42] J.P. Meyer, M. Everts, Single-phase mixed convection of developing and fully developed flow in smooth horizontal circular tubes in the laminar and transitional flow regimes, Int. J. Heat Mass Transf. 117 (2018) 1251–1273.
[43] M. Everts, J.P. Meyer, Relationship between pressure drop and heat transfer of developing and fully developed flow in smooth horizontal circular tubes in the laminar, transitional, quasi-turbulent and turbulent flow regimes, Int. J. Heat Mass Transf. 117 (2018) 1231–1250.
[44] C. Zhou, Y. Yao, L. Ni, Development of heat transfer correlations for multi-row helically coiled tube heat exchangers used in surface water heat pump systems, Int. J. Heat Mass Transf. (2020) 163.
[45] Y. Qu, L. Wang, X. Lin, H. Ling, Y. Bai, S. Zhang, H. Chen, Heat transfer characteristics of mixed convection in packed beds, Chem. Eng. Sci. (2022) 255.
[46] C.W. Hollingshead, A. Rashkovan, D.R. Novog, Mixed convection around two vertically aligned horizontal cylinders: a numerical, experimental, and modeling investigation on the effect of local conditions on heat transfer, Nucl. Eng. Des. (2022) 394.
[47] E. Lemmon, M.L. Huber, M.O. McLinden, NIST standard reference database 23: reference fluid thermodynamic and transport properties-REFPROP, version 8.0, (2007).
[48] H. Kallath, F.K. Kholi, Q. Jin, M.Y. Ha, S.H. Park, H.-j. Kim, J. Chetwynd-Chatwin, J.K. Min, Numerical Study of the Flow Uniformity Inside the High-Pressure Side Manifolds of a Cooled Cooling Air Heat Exchanger, Appl. Therm. Eng. (2021) 189.
[49] N. Hasan, B. Farouk, Fast heating induced thermoacoustic waves in supercritical fluids: experimental and numerical studies, J. Heat Transf. 135 (8) (2013).
[50] A. Fluent, Version 15.0: User Manual, ANSYS, Inc., Canonsburg, USA, 2013.
[51] A. Bejan, Convection Heat Transfer, John wiley & sons, 2013.
[52] J. Dyer, The development of laminar natural-convective flow in a vertical uniform heat flux duct, Int. J. Heat Mass Transf. 18 (12) (1975) 1455–1465.